

Ab initio study of the β -tin \rightarrow *Imma* \rightarrow sh phase transitions in silicon and germanium

Katalin Gaál-Nagy, Pasquale Pavone, and Dieter Strauch

Institut für theoretische Physik, Universität Regensburg, D-93040 Regensburg, Germany

(Dated: November 8, 2018)

We have investigated the structural sequence of the high-pressure phases of silicon and germanium. We have focussed on the cd \rightarrow β -tin \rightarrow *Imma* \rightarrow sh phase transitions. We have used the plane-wave pseudopotential approach to the density-functional theory implemented within the Vienna *ab-initio* simulation package (VASP). We have determined the equilibrium properties of each structure and the values of the critical parameters including a hysteresis effect at the phase transitions. The order of the phase transitions has been obtained alternatively from the pressure dependence of the enthalpy and of the internal structure parameters. The commonly used tangent construction is shown to be very unreliable. Our calculations identify a first-order phase transition from the cd to the β -tin and from the *Imma* to the sh phase, and they indicate the possibility of a second-order phase-transition from the β -tin to the *Imma* phase. Finally, we have derived the enthalpy barriers between the phases.

PACS numbers: 61.50.Ks, 64.70.Kb, 71.15.Nc, 71.20.Mq, 81.30.Dz, 81.40.Vw

I. INTRODUCTION

Although the structural sequence of the high-pressure phase transitions in Si and Ge has been considered to be well known since two decades, a new high-pressure phase was found experimentally between the body-centered tetragonal structure with two basis atoms (which will be referred to the following as β -tin or BCT phase) and the simple-hexagonal (sh) structure in Si^{1,2} and Ge.^{3,4} After its space group this intermediate phase was called *Imma* phase and corresponds to a body-centered orthorhombic Bravais lattice with two atoms in the unit cell (which will be called in the following BCO). Thus, the experimental structural sequence is found to be cd \rightarrow β -tin \rightarrow *Imma* \rightarrow sh \rightarrow ..., where cd indicates the cubic-diamond structure. A BCO structure was first theoretically proposed for Si by Needs and Martin⁵ about twenty years ago, whereas Lewis and Cohen⁶ predicted exactly the *Imma* phase for Ge a few years before the experimental confirmation. The first theoretical investigations for Si and Ge indicated for both, the β -tin \rightarrow *Imma* and the *Imma* \rightarrow sh case, a continuous second-order phase transition.^{6,7} At variance, the experiments show first-order phase transitions with a discontinuity of the volume in both substances and a hysteresis effect in Si.² For Ge the first-order transition was detected only for the β -tin \rightarrow *Imma* transition,³ because the *Imma* \rightarrow sh transition was expected to be beyond the experimentally accessible pressure range. The transition pressures in Ge are expected to be higher than the corresponding ones in Si, because of the strong repulsive character of the atomic potential in Ge due to the presence of *d* electrons in the core.⁸ From the theoretical point of view, recent total-energy calculations show two first-order phase transitions β -tin \rightarrow *Imma* and *Imma* \rightarrow sh both for Si⁹ and Ge.¹⁰ A second-order phase transition was found for the β -tin \rightarrow *Imma* case from elastic instabilities.¹¹

First information on the order of the phase transition can be given by group-theoretical arguments:¹² If the or-

der of the point group of one phase is one half of the order of the point group of the other phase, then the phase transition can be of second order. If the point group of one phase is one third of the order of the point group of the other phase, then the phase transition must be of first order. The order of the point group $m\bar{3}m$ of the cd structure (space group O_h^7 , $Fd\bar{3}m$) is 48. Since the order of the point group $4/mmm$ of the β -tin phase (space group D_{4h}^{19} , $I4_1/amd$) is 16, the cd \rightarrow β -tin transition has to be of first order. The order of the point group mmm of the *Imma* phase (space group D_{2h}^{28} , *Imma*) is 8, thus the β -tin \rightarrow *Imma* transition can be a second-order one. Furthermore, the order of the point group $6/mmm$ of the sh structure (space group D_{6h}^1 , $P6/mmm$) is 24, the sh \rightarrow *Imma* and also the *Imma* \rightarrow sh transitions are of first order. Following the group-theoretical analysis none of the available total-energy calculations have described correctly the order for the phase transitions of the whole sequence, neither for Si nor for Ge.

This paper is organised as follows: In Section II we give a short overview of the methods on which our calculations are based. In Section III we report the results for the equilibrium parameters of these phases and compare them with the experimental volume dependence. Transition pressure ranges are presented in Section IV. The order of the phase transitions is analysed in Section V, and the enthalpy barriers between the phases are determined in Section VI. All results are summed up and discussed in Section VII. The conclusions are summarised in Section VIII.

II. METHOD

Our calculations have been performed using the plane-wave pseudopotential approach to the density-functional theory (DFT)^{13,14} implemented within the Vienna *ab-initio* simulation package (VASP).¹⁵ For the exchange-correlation potential we have used the generalised-

gradient approximation (GGA) by Perdew and Wang¹⁶ for Si and Ge, and, because of poorer results, the local-density approximation (LDA)^{17,18} for Si only. The interaction with the ion cores has been described by ultrasoft pseudopotentials.^{19,20} The wave functions have been expanded in terms of plane waves up to a kinetic-energy cutoff of 270 eV (410 eV) for Si (Ge). This choice provided an error smaller than 0.5 kbar (0.2 kbar) for Si (Ge) to the pressure according to the Pulay stress.²¹ The Pulay stress arises from using an incomplete plane-wave basis set and causes errors in the stress tensor and, correspondingly, in the pressure. Convergence also required a $18 \times 18 \times 18$ ($24 \times 24 \times 24$) mesh of Monkhorst-Pack points²² which yielded 864 (1962) \mathbf{k} -points in the irreducible wedge of the Brillouin zone for Si (Ge). All high-pressure phases are metallic. Thus, we have used a Methfessel-Paxton smearing²³ with a width of 0.2 eV. In order to determine the total energy for a given volume or structure we have minimised the energy with a conjugate-gradient algorithm.^{24,25,26} The equilibrium properties have been obtained by fitting the values of the energy as a function of the volume alternatively to the Vinet²⁷ and to the Murnaghan²⁸ equation of state.

III. STRUCTURAL RELAXATION AND EQUILIBRIUM PROPERTIES

In this section we present our results for the volume dependence of the structural parameters and compare them with the experimental ones. The structural parameters are more useful indicators of phase transitions than the often-used tangent construction to the equation-of-state curves, the difficulties of which will be illuminated.

We have focussed our attention to the structural sequence β -tin \rightarrow Imma \rightarrow sh. The calculations for the cd phase have been performed just for the sake of comparison. The most general structure which is compatible with all four phases is the body-centered orthorhombic cell with a basis of two atoms at $(0,0,0)$ and $(0,0.5b, \Delta c)$ (BCO structure). The other structures are special cases: For the BCT structure (β -tin) one has the lattice constants $a = b$ and the internal parameter $\Delta = 0.25$; for the sh structure one has $b = \sqrt{3}c$ and $\Delta = 0.5$; for the cd phase one has $b = a$, $c = \sqrt{2}a$, and $\Delta = 0.25$. The pure Imma phase is realised as a BCO structure with $a \neq b \neq c \neq a$ and $0.25 < \Delta < 0.5$. The minimization of the total energy has been performed using the following procedure: For all phases we have started from the BCO structure and minimised the energy as a function of the structural parameters with the constraints appropriate to the various phases. In this way we have avoided an energy offset which arises from using different cells. For example, in the case of the cd structure we have imposed, according to the previous considerations, $b = a$, $c = \sqrt{2}a$, and $\Delta = 0.25$, and then we have minimised the total energy as a function of a . In the special case of the sh structure, we could keep only the value of Δ fixed at 0.5, and

we have relaxed the value of b/c (and also c/a) by minimization of the energy; the structure which is obtained after relaxation will be indicated in the following as SH. Indeed, converged calculations should yield $b/c = \sqrt{3}$ (SH = sh) after relaxation. For the Imma phase, all lattice and internal parameters of the BCO structure were allowed to relax.

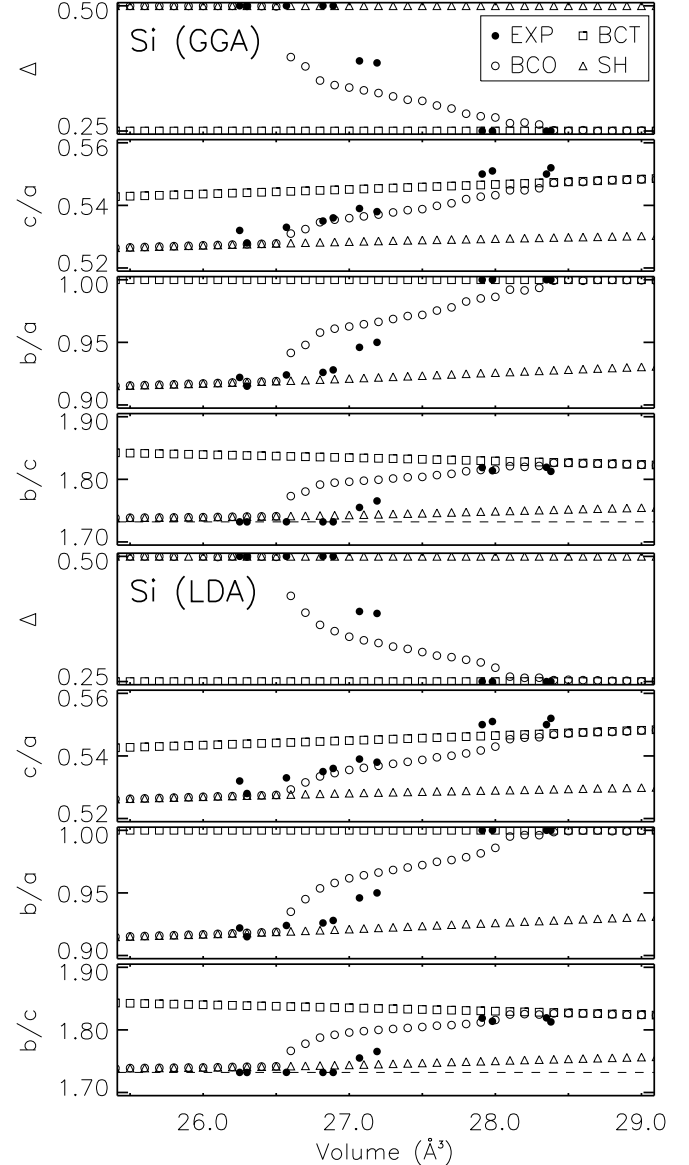


FIG. 1: Volume dependence of the structural parameters of the BCT, BCO, and SH structures for Si within GGA (upper panels) and LDA (lower panels). The dashed line indicates the ideal value of $b/c = \sqrt{3}$. The experimental data are taken from Refs. 1,2,30,31,32.

The relaxed parameters as a function of the volume are displayed in Figs. 1 and 2 for Si and Ge, respectively. The results from calculations performed with the GGA and the LDA are quite similar for Si. Since it turned out, that the pressures calculated by GGA are more accurate

in Si, only GGA calculations have been performed for Ge. As can be seen in Fig. 1, the relaxation of b/c for the SH phase of Si does not match the ideal value. At variance, the calculation for Ge does reproduce this value. This indicates that for a full convergence a higher kinetic-energy cutoff and/or a larger grid of special points should have been used for Si. However, the condition $b/c = \sqrt{3}$ is almost fulfilled in the region of stability of the sh phase. Furthermore, the energy obtained from a calculation in the same cell with $b = \sqrt{3}c$ fixed and c/a relaxed differs from the value obtained using the previous procedure by less than 0.7 meV. For a more detailed discussion see Ref. 29.

The agreement between our data and those experimental ones which are not included in the figure is good: The reported value of $c/a = 0.552$ for the β -tin phase of Si³³ is well within the range of our values. The experimental values of $b/a = 0.917$ and $c/a = 0.530$ at the volume $V = 24.43 \text{ \AA}^3$ of Ref. 34 agree with our data. Furthermore, the measured value of 24.22 \AA^3 for the volume of the sh phase of Si³⁵ is also in the stability range we have found for this phase. For Ge in the BCT structure, a c/a ratio of 0.548–0.554 was detected experimentally^{32,36,37,38,39} corresponding to a volume region around 33 \AA^3 ; in this region, our c/a ratio is 0.546–0.549. For the sh phase of Ge, a b/a ratio of 0.93 was measured³⁹ which also agrees with our data.

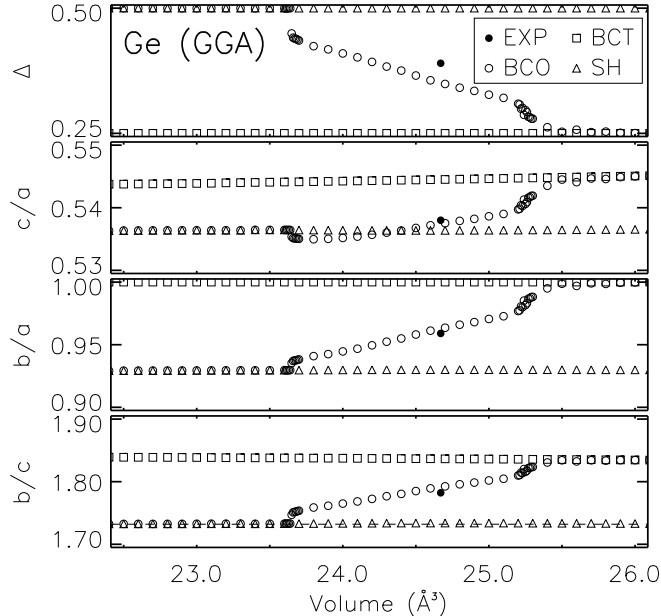


FIG. 2: The same of Fig. 1 for Ge within GGA. The experimental data are taken from Ref. 3.

Figures 1 and 2 show that the relaxation of the general BCO structure leads to the BCT structure for large volumes and to the SH structure for small ones. In the intermediate region, extending from about 26.5 to 28.0 \AA^3 for Si and 23.5 to 25.5 \AA^3 for Ge, we localise the stability range of the pure *Imma* phase. Whereas the transi-

tion between the *Imma* and the sh phase is characterised by a discontinuity in most of the structural parameters, the *Imma* and the β -tin phase are quite difficult to distinguish by an inspection of Figs. 1 and 2. A clearer picture is obtained from the electronic structure and the Fermi energy (see Appendix A for details). From this procedure, the stability range of the *Imma* phase is from 26.6 to 28.3 \AA^3 for Si (GGA), from 26.6 to 28.0 \AA^3 for Si (LDA), and from 23.7 to 25.4 \AA^3 for Ge.

The standard procedure for calculating the volume change and the pressure at the transition is the so-called common-tangent construction. It relies on the fact that, in the case of a first-order phase transition, two structures with the same pressure p and enthalpy H but different total energy $E(V)$ coexist. The volume derivative of the total energy is the negative pressure. Therefore, the slope of the common tangent to the two energy curves gives the pressure for the transition between the corresponding structures. Due to the fact that calculations are performed at a finite number of volumes, a fit of an analytical expression to a continuous energy curve is needed in order to obtain a continuous derivative.

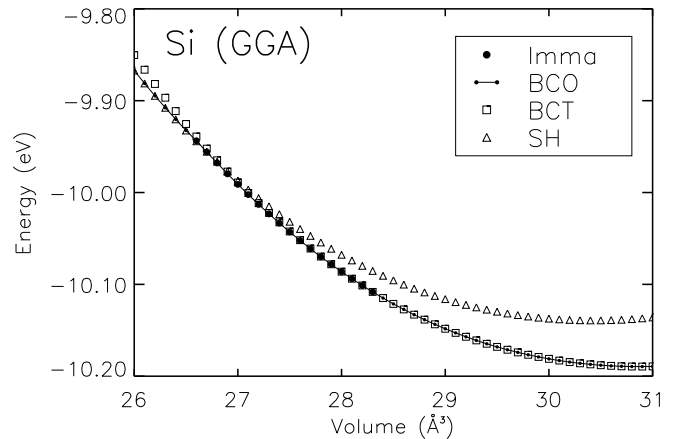


FIG. 3: Energy vs. volume for the involved structures of Si within GGA (see text for explanation).

In Fig. 3 we show the energy of the relaxed structures for Si as a function of volume. The volume region where the pure *Imma* phase is stable does not include any minimum of the total energy E . This makes a fit to any equation of state for the *Imma* phase slightly unstable, which results in an unreliable determination of the transition pressures and of the volume change through the common-tangent construction in this region. The results from a fit of the Vinet²⁷ and Murnaghan²⁸ equation of state are shown in Table I for Ge as well as a comparison of the LDA and GGA calculations for Si.

Typically, the GGA tends to overestimate the equilibrium volume whereas the LDA tends to underestimate it. For the cd phase of Si the experimental equilibrium volume at room temperature is^{1,40,41,42,43} 40.05 \AA^3 , which lies between the LDA and GGA ones, with a deviation of about 2%. The experimental value for cd Ge is^{37,42,44,45}

TABLE I: Equilibrium parameter determined by the Murnaghan (Mur) and Vinet (Vin) equation of state for the cd, β -tin, *Imma*, and sh phase of Si and Ge. The equilibrium volume V_0 is in units of \AA^3 and the bulk modulus B_0 in kbar.

	Si-GGA		Si-LDA		Ge-GGA	
	Mur	Vin	Mur	Vin	Mur	Vin
cd	V_0	40.65	40.61	39.18	39.14	47.75
	B_0	892	883	949	956	584
	B'_0	3.67	4.21	3.77	4.16	4.75
β -tin	V_0	30.86	30.87	29.59	29.58	38.85
	B_0	1067	1041	1163	1159	720
	B'_0	3.87	4.46	3.99	4.36	3.77
<i>Imma</i>	V_0	31.45	31.54	30.22	30.05	39.03
	B_0	795	792	799	874	805
	B'_0	4.94	4.98	4.97	4.89	3.31
sh	V_0	30.42	30.43	29.12	29.11	38.77
	B_0	1030	1012	1135	1137	768
	B'_0	4.05	4.61	4.20	4.52	3.50

between 45.00 and 45.31 \AA^3 , with a deviation from our result of less than 6%. Because the other phases exist only under pressure, experimental values do not exist to which our equilibrium parameters could be compared.

If the standard common-tangent construction is used in order to extract the transition parameters, an accurate determination of both, equilibrium volumes and curvature of the energy vs. volume curve, is needed. This applies even more so in the present case in which $E(V)$ curves and equilibrium volumes of the β -tin, *Imma* and sh phases are very close together. Even though the present calculation are numerically involved the resulting data of Table I are not precise enough. For example, in all calculations (LDA and GGA) for Si the fitted (Vinet and Murnaghan) energy curves of the *Imma* phase fall below the ones of the β -tin phase, even for large volumes. In these cases the *Imma* phase is more stable than the β -tin phase. Thus, within this construction either a phase transition from the cd to the β -tin phase can be observed, if one neglects the *Imma* phase, or a phase transition from the cd to the *Imma* phase can be observed without a locally stable β -tin phase. A direct transition from the β -tin to the *Imma* phase cannot be detected. Similar drawbacks are found for Ge. Furthermore, the method is applicable only to the investigation of first-order phase transitions. For all these reasons, it is very difficult to extract the reliable information on the transitions using the tangent construction. In the following section, we consider an alternative procedure for analysing the transitions which does not contain the drawbacks of the above one.

IV. DETERMINATION OF THE TRANSITION PRESSURES AND HYSTERESIS EFFECT

In this section we present results for the pressure dependence of the structural parameters in order to give an estimate of the transition pressures by considering the stability range of the *Imma* phase.

The pressure p in a crystal can be directly calculated from the stress tensor σ . Within the BCO structure the off-diagonal components of the stress tensor vanish. Therefore, the most general form of the stress tensor of our structures is

$$\sigma = - \begin{pmatrix} p_x & & \\ & p_y & \\ & & p_z \end{pmatrix} . \quad (1)$$

The results of the previous section correspond to hydrostatic pressure

$$p = p_x = p_y = p_z , \quad (2)$$

and, in our results of Section III, Eq. (2) is fulfilled within an error of 0.1 kbar for Si and 0.05 kbar for Ge, which is less than the pressure error due to the Pulay stress. For each of the relaxed BCO structures as described in Section III, we have calculated the hydrostatic pressure corresponding to the structural parameters as shown in Figs. 1 and 2. The pressure dependence of the structural parameters is presented in Figs. 4 and 5. There is a clear discontinuity of the parameters of the *Imma* phase and the sh phase. The values of the parameters of the pure *Imma* phase are highlighted as special values of the relaxed BCO structure. For both Si and Ge, the β -tin \rightarrow *Imma* phase transition seems to be continuous. For Si, the relaxed parameters calculated within LDA and GGA are very similar, but the corresponding pressures differ as shown in Fig. 4. In contrast, the volume range of stability in both cases is similar (see Fig. 1). Usually, the GGA transition pressures are closer to the experimental ones than the LDA values. Therefore, we will focus in the following mainly on the GGA results.

The assignment of the phases from the data points in Figs. 4 and 5 are taken from Section III. In the case of the GGA calculation for Si we have found the following sequence with pressure increase: For the β -tin \rightarrow *Imma* phase transition, the transition pressure is approximately between 104 (last relaxation of the system to a BCT structure) and 109 kbar (first relaxation of the system to a BCO structure with $\Delta \neq 0.25$). The next transition is the one from the *Imma* to the sh phase. As can be seen in Figs. 4 and 5, there is an overlap of different structures for certain values of the pressure, which can be interpreted as a hysteresis effect. That means that the transition value for increasing and decreasing pressure is different. This effect was first observed first in the experiment for Si.² We estimate the hysteresis effect for Si as follows: The last appearance of the pure *Imma* phase ($\Delta \neq 0.5$) without any SH structure at the same pressure

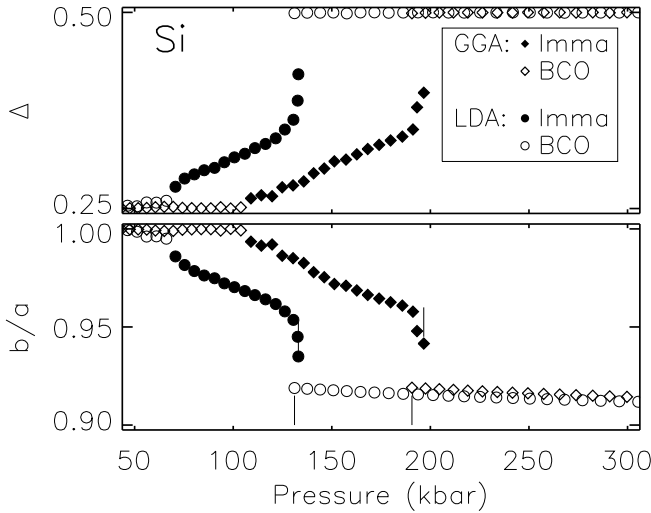


FIG. 4: Dependence of the structural parameters Δ and b/a on the hydrostatic pressure for the relaxed phases for Si with GGA (full and empty diamonds) and LDA (full and empty circles). The range of the pressure hysteresis of the overlapping phase regions are marked by vertical lines.

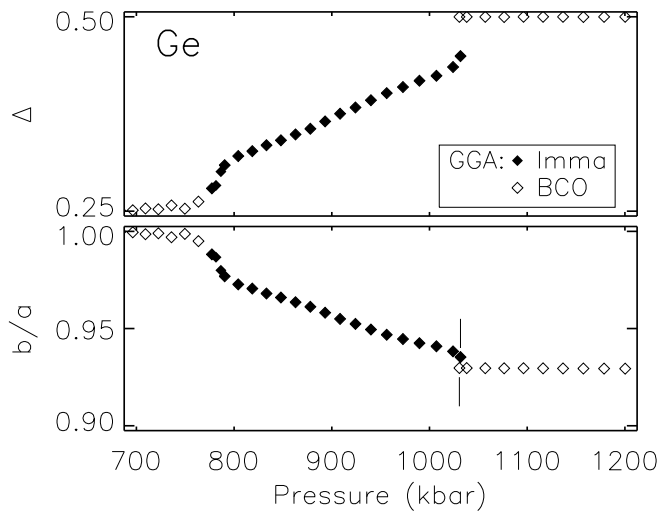


FIG. 5: The same of Fig. 4 but for Ge for GGA only.

is at 186 kbar, the first appearance of the sh phase is at 191 kbar (downstroke), the last appearance of the pure *Imma* phase is at 197 kbar and the first appearance of the sh structure *without* any parallel *Imma* phase is at 198 kbar (upstroke). The transition pressures estimated in this way are listed in Table II.

Since we have calculated the lowest energy structure, the values in Table II give an estimate of the hysteresis effect. An alternative approach to the hysteresis effect will be described in Section VI.

TABLE II: Summary of the estimated transition pressures at increasing (\uparrow) and decreasing (\downarrow) pressure for the phase transitions between the β -tin, *Imma* and sh phase.

Si			transition pressure (kbar)	
β -tin	\leftrightarrow <i>Imma</i>		GGA 104–109 ($\uparrow\downarrow$)	
	LDA 66–71 ($\uparrow\downarrow$)			
<i>Imma</i>	\leftrightarrow sh		197–198 (\uparrow)	186–191 (\downarrow)
	LDA 133–138 (\uparrow)		131 (\downarrow)	
Ge				
β -tin	\leftrightarrow <i>Imma</i>		GGA 750–763 ($\uparrow\downarrow$)	
	<i>Imma</i>		1032 (\uparrow)	1031–1029 (\downarrow)

V. ORDER OF THE PHASE TRANSITIONS

The thermodynamical potential for a pressure-induced phase transition is the Gibbs free energy. Neglecting temperature effects, the Gibbs free energy is equal to the enthalpy $H = E + pV$. For calculating the enthalpy, we have used the energy $E(V)$ of the relaxed structures with a volume V and the hydrostatic pressure p from Eq. (2).

At a given pressure, the stable structure is the one with the lowest enthalpy. Therefore, the transition pressure p_t for a transition $A \rightarrow B$ is defined by $H^A(p_t) = H^B(p_t)$. For a first-order phase transition the enthalpy curves $H^A(p)$ and $H^B(p)$ of the two phases cross at p_t , and their derivatives dH/dp at p_t are different for the two phases. For a second-order transition, the second derivatives of the enthalpy curves at p_t for the two phases are different, whereas the first derivatives are equal. In this case the corresponding enthalpy curves have a boundary point at p_t .

In the following, we analyse the transitions in order to extract the corresponding transition pressure and order. The enthalpy $H(p)$ and its first derivative are presented in Fig. 6 for Ge. The enthalpy curves have been reduced by the value of the BCT structure for the β -tin \rightarrow *Imma* transition,

$$\Delta H(p) = H(p) - H^{\text{BCT}}(p) \quad (3)$$

and by the value of the SH structure for the *Imma* \rightarrow sh transition,

$$\Delta H(p) = H(p) - H^{\text{SH}}(p) \quad . \quad (4)$$

The derivative indicated by black dots in the lower panels of Fig. 6 has been calculated by finite differences, the straight solid line is a linear fit of these data, obtained by using only points belonging to the numerically stable regime (790–1030 kbar). An integration of this linear function is fully consistent with the enthalpy values in the upper panels. The enthalpy differences of the points in the pressure range $p < 790$ kbar stem from the numerical noise of our calculation.

For the *Imma* \rightarrow sh transition (right panels of Fig. 6) the two enthalpy curves cross at the transition pressure $p_t =$

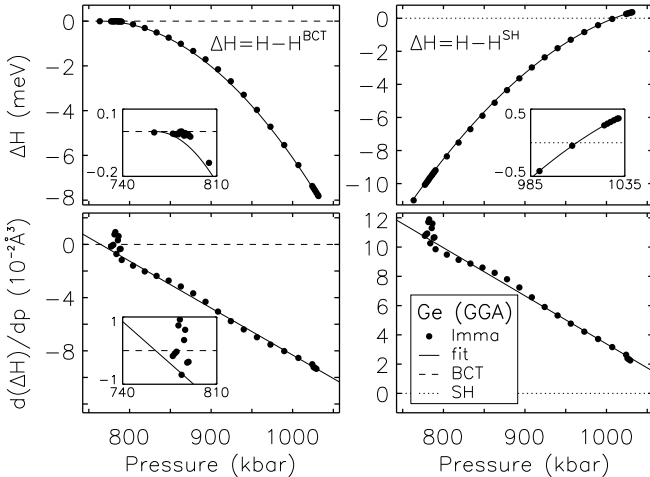


FIG. 6: Enthalpy vs. pressure (upper panels) and derivative of the enthalpy vs. pressure (lower panels) for Ge reduced by the corresponding curves of the BCT (right panels) and the SH (left panels) structure. The solid lines are quadratic (upper panels) and linear (lower panels) fits.

1009 kbar. Therefore, this phase transition is clearly of first order. The change of the derivatives at the transition point is the volume change $\Delta V(p_t)$ and can be directly read from the lower panel of Fig. 6.

For β -tin \rightarrow *Imma* (left panels of Fig. 6) the enthalpy curves are very close to each other in the region where the phase transition is expected. From this point of view, transitions of both first and second order are conceivable. We have thus analysed our data assuming alternatively a first- and a second-order transition.

Assuming a second-order transition the transition pressure is obtained by looking at the crossing of the dH/dp curves.

A precise value of the β -tin \rightarrow *Imma* transition pressure assuming first order can not be determined by a crossing of the enthalpy curves due to the numerical accuracy of our calculation. We are only able to give a rough estimate of the pressure at which the transition can occur due to an extrapolation of the more reliable data points away from the transition pressure. The results for Si have been obtained in an analogous way.

For both Si and Ge, the values of p_t and of the volume changes between the low- and the high-pressure phase are shown in Table III.

For Si the volume changes ΔV for an assumed first-order β -tin \rightarrow *Imma* transition from LDA and from GGA and are very small compared to the changes for *Imma* \rightarrow sh. Thus we conclude that the phase transition β -tin \rightarrow *Imma* in Si most probably is of second order.

For Ge the volume changes for a first-order β -tin \rightarrow *Imma* and *Imma* \rightarrow sh transition are within the same range. The value of $p_t = 792$ kbar is higher than the ones from the estimated range (750–763 kbar) of the previous section, and overestimating p_t results in overestimating ΔV . A reason for the large value of p_t can be found in the

TABLE III: Transition pressure (p_t), order (ord), and volume change (ΔV) for Ge from Fig. 6 and similarly for Si.

	ord	p_t (kbar)		ΔV (m \AA^3)	
		GGA	LDA	GGA	LDA
cd \rightarrow β -tin	Si	1	121	79	8136
	Ge	1	96	–	7508
β -tin \rightarrow <i>Imma</i>	Si	2	108	65	0
	Si	1	103	71	-1.2
	Ge	2	765	–	0
	Ge	1	792	–	9.5
<i>Imma</i> \rightarrow sh	Si	1	189	127	301.4
	Ge	1	1009	–	30.7

fact, that the last reliable data points are too far away from the region where the phase transition is expected to occur. Thus, it is not possible to decide whether the transition β -tin \rightarrow *Imma* is of first or of second order. Because of the similarities of Si and Ge a second-order transition seems more probable. If this phase transition is a discontinuous one, it is at least weakly of first order.

Using the enthalpy method the transition pressure for cd \rightarrow β -tin in Si is calculated to be larger than the one for the β -tin \rightarrow *Imma* transition. These two phase transitions take place in a small pressure range and therefore numerical errors in the determination of the transition pressure may lead to a wrong sequence. See the discussion at the end of Section III.

VI. ENERGY SURFACES AND ENTHALPY BARRIERS

In this section, we present the results for the energy surfaces for Ge (similar calculations have been done for Si) as well as for the enthalpy barriers for the cd \rightarrow β -tin and *Imma* \rightarrow sh transitions.

We have obtained the energy surface by calculating the energy corresponding to given values of the parameters V , b/a , and c/a and a relaxed internal parameter Δ . On the energy surface the pressure is non-hydrostatic except one or two lines or a few points. Next, we consider the pressure defined in Eq. (2) in the non-hydrostatic case

$$p_0 = \frac{1}{3} (p_x + p_y + p_z) \quad (5)$$

where $-p_x$, $-p_y$, and $-p_z$ are the components of the diagonal stress tensor, Eq.(1).

For every first-order phase transition, there exists an energy barrier which has to be overcome on the path from the one phase to the other. For most reactions, such as, e.g., adsorption processes, it is a barrier of the total energy E which lies between two local minima in the corresponding energy space. For this kind of transition, the reaction path and the energy barrier between

the two phases can be found by using, e.g., the nudged-elastic-band method,^{46,47} by which the lowest energy path between two local minima is detected. However, this method requires the existence of well-defined local energy minima corresponding to the two phases.

If the transition, for instance the one from the cd to the β -tin phase in Ge, would occur without any influence of pressure, the corresponding energy space would be the energy surface $E(V, c/a)$ drawn in Fig. 7. The reaction coordinate here is taken as c/a . As expected, there are two local minima and a saddle point between them. By symmetry, the condition $p_x = p_y$ is valid all over the energy surface. The energy minima and the saddle point lie on the contour line $p_x = p_z$, which indicates the hydrostatic condition. The energy barrier is then defined as the energy difference between the saddle point and the starting minimum.

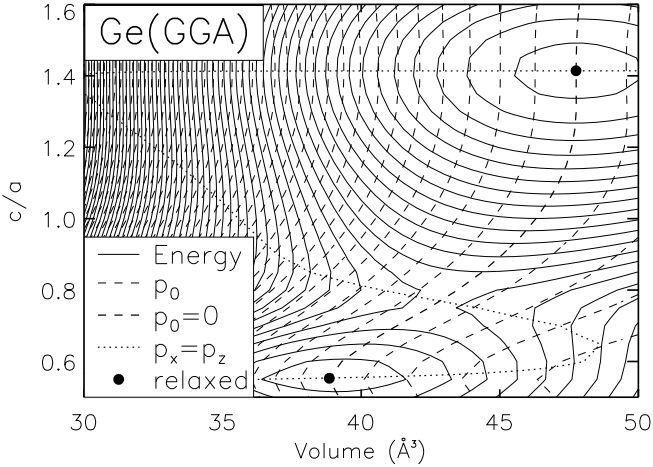


FIG. 7: Contour plot of the total energy $E(V, c/a)$ and of the average pressure $p_0(V, c/a)$ (see Eq. 5) for Ge. The interval of the contour lines is 50 meV for the energy and 20 kbar for the pressure surfaces. The conditions $p_x = p_y$, $b/a = 1$, and $\Delta = 0.25$ are fulfilled within the whole area. The black dots mark the equilibrium positions of the cd ($c/a = \sqrt{2}$) and the β -tin phase ($c/a = 0.55$). The dotted line marks the parameters under hydrostatic condition.

However, in our case the phase transition is driven by the pressure, and therefore the associated thermodynamical potential is the Gibbs free energy or the enthalpy, if temperature effects are neglected. The enthalpy surface corresponding to the cd and β -tin phases for Ge is shown in Fig. 8. The enthalpy for each set of parameters $(V, c/a)$ is calculated as $H(V, c/a) = E(V, c/a) + V p_0(V, c/a)$. In the range displayed in Fig. 8 the enthalpy surface has no minimum. Therefore, the usual path methods are not applicable here. However, the enthalpy barrier can be calculated in a different way as follows: The phase transition between the A and B phases occurs at the pressure p_t at which $H^A(p_t) = H^B(p_t)$. Hence, we have to look for the points along the isobars in Fig. 8 which have the same value of the enthalpy.

In order to visualise the enthalpy barrier, we draw in

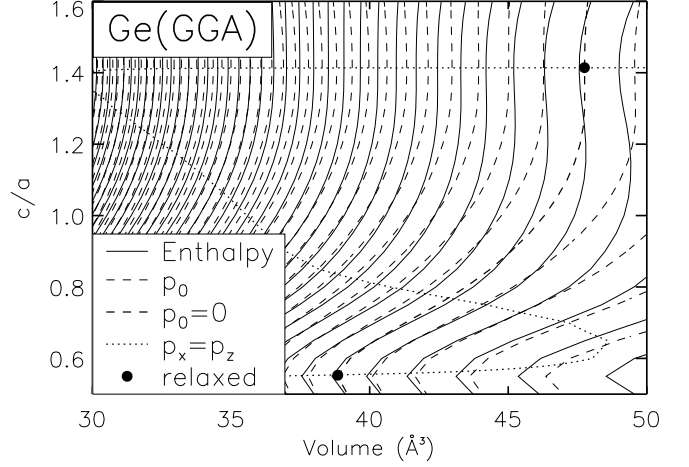


FIG. 8: Same as Fig. 7 but for the enthalpy $H(V, c/a)$ of Ge. The interval between the contour lines for H is 500 meV.

Fig. 9 the enthalpy at constant average pressure (with $p_x = p_y$) as a function of the reaction coordinate c/a . For convenience the enthalpy is reduced by the starting point with $c/a = \sqrt{2}$,

$$\Delta H(c/a) = H(c/a) - H(\sqrt{2}) , \quad (6)$$

which determines here the cd structure. As can be seen in Fig. 9, there exists just one enthalpy line at constant pressure, which touches the zero line twice according to $H^A(p) = H^B(p)$. The corresponding pressure is the transition pressure p_t and the height of the maximum between these minima is the height of the enthalpy barrier for this phase transition. Note that on the isobars at most three points refer to hydrostatic pressure, while the other points corresponds just to the condition $p_x = p_y$.

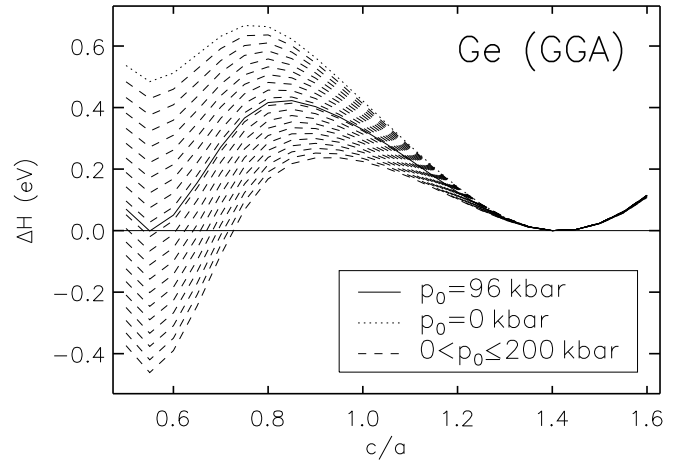


FIG. 9: Enthalpy difference at constant average pressure vs. the reaction coordinate c/a , see Eq. (6) for Ge. The solid line is for the cd \rightarrow β -tin transition pressure. The pressure interval between consecutive lines is 10 kbar.

Similar pictures can be drawn for the cd \rightarrow β -tin transition of silicon. The height of enthalpy barrier is found

to be 423 meV for Ge within GGA and 515 and 508 meV for Si within GGA and LDA, respectively. In agreement with previous results,⁴⁸ the barrier for Ge is smaller than for Si.

For the $cd \rightarrow \beta$ -tin phase transition the determination of the enthalpy barrier is easy because only the volume and the c/a ratio can vary, and the latter can be used as the reaction coordinate. For the β -tin \rightarrow $Imma \rightarrow sh$ transition all the parameters c/a , b/a , b/c , and Δ are changing (but only two of the ratios are independent). We have calculated the total energy for each set of parameter $(V, c/a, b/a)$, the internal parameter Δ has been relaxed for each set. Selected energy contour plots at constant volume are presented in Fig. 10. In these plots, the places where two of the diagonal components of the stress tensor are equal are explicitly shown by the dotted, dashed, and dash-dotted lines. Obviously, hydrostatic condition is indicated by the points where all of these lines cross. Different hydrostatic pressures at one volume (like at $V = 24 \text{ \AA}^3$) can lead to a multivalued pressure-volume relation.

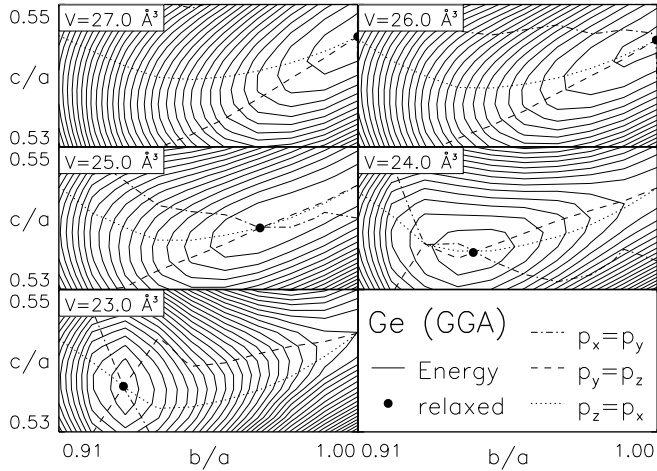


FIG. 10: Contour plots of the total energy $E(b/a, c/a)$ for selected volumes noted in the insets for Ge. The interval of the contour lines is 1 meV. The black dots mark the equilibrium positions. The hydrostatic condition is produced by the crossing of all the lines $p_x = p_y$, $p_y = p_z$, and $p_z = p_x$.

In order to calculate the enthalpy barrier in analogy to the $cd \rightarrow \beta$ -tin transition, we present a contour plot of the enthalpy as a function of the volume V and of the b/a ratio in Fig. 11. Actually, the enthalpy depends also on the other variables c/a and Δ . The contour plot of Fig. 11 has been obtained using the following procedure: For each value of the set $(V, b/a)$, we have chosen c/a so as to fulfill the condition $p_z = p_x$ (see Fig. 10), which is suggested because at the end we will look for the points which fulfill the hydrostatic condition. The value of Δ has been taken so as to minimise the energy for a given choice of the other parameters. The two-dimensional presentation of the results as in Fig. 11 corresponds to the choice of b/a as the reaction coordi-

nate. Completely equivalent results can be obtained by choosing c/a or Δ instead. The hydrostatic condition in Fig. 11 is then realised by $p_y = p_z$.

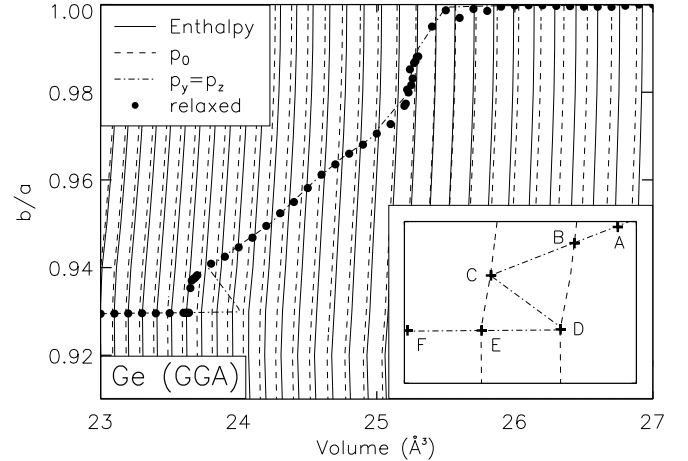


FIG. 11: Contour plot of the enthalpy $H(V, b/a)$ and of the pressure $p_0(V, b/a)$ for Ge. The interval of the contour lines is 300 meV for the enthalpy and 20 kbar for the pressure increasing from right to left. The condition $p_x = p_z$ is fulfilled within the whole area. The dash-dotted line reproduce the hydrostatic condition. The inset shows the schematical behavior between 23.5 and 24 \AA^3 , see text.

The comparison with our previous results shows that most of the data shown in Fig. 5 lie on the hydrostatic line. Numerical instabilities lead to deviations (generally of less than 1 kbar) between the relaxed points and the line $p_y = p_z$. Nevertheless, the relaxed points show the same behaviour (to a lesser extent) as the hydrostatic line, which is shown schematically in the inset of Fig. 11.

The schematical behaviour of the hydrostatic curve between approximately 23.5 and 24 \AA^3 as shown in the inset of Fig. 11 can be used to discuss the hysteresis effect qualitatively. If one follows the hydrostatic line $p_y = p_z$ with increasing pressure p (decreasing volume) starting from A, one arrives at the point C where the direction of the line is changing. From C to D, the pressure decreases with a simultaneous decrease of the volume which is an unstable situation. Thus, at C the phase transition must occur through a jump from C to E, which is at the same pressure. From E increasing pressure leads to F. Following the path in the opposite direction starting from F, i.e., by decreasing the pressure (volume increase), the direction of the curve changes at D, which results in a jump to B. As a consequence of that it is possible to have a higher transition pressure with increasing than with decreasing pressure. Therefore, an alternative estimate for the limit of the hysteresis effect can be given. For Si within GGA (LDA), we obtain a transition pressure of 198 (133) kbar with increasing and of 169 (109) kbar with decreasing pressure. For Ge within GGA, the corresponding values are 1010 and 965 kbar.

A behaviour similar to the one depicted in the inset of Fig. 11 can be found also for the $cd \rightarrow \beta$ -tin phase tran-

sition (see Fig. 8). There, the low-pressure edge corresponding to the point C of the inset of Fig. 11 is at a negative pressure, which would lead for β -tin \rightarrow cd to a very low or even negative transition pressure, the latter case being connected to the irreversibility of the phase transition. For the cd \rightarrow β -tin transition the volume and the enthalpy as a function of hydrostatic pressure is presented in Fig. 12. The values have been extracted from Fig. 8 along the hydrostatic line $p_x = p_z (= p_y)$. The ideal cd structure ($c/a = \sqrt{2}$) has been reached within an error of 1% and therefore cd is noted as CD in analogy to the difference between sh and SH (see Section III). In order to discriminate the enthalpy curves of Fig. 12 we have subtracted a linear background to arrive at the curves ΔH . The solid and the dashed line mark the CD and the BCT structure, respectively. The dotted line indicate the values along the part of the hydrostatic line, which connects the CD and the BCT structure. The designated points correspond to the inset of Fig. 11.

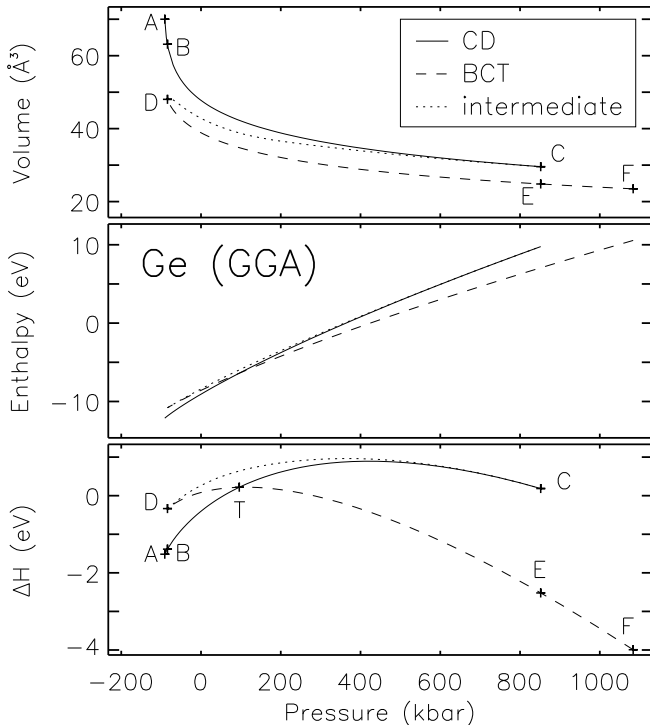


FIG. 12: Volume, enthalpy and reduced enthalpy vs. hydrostatic pressure for Ge. The points noted in the figures correspond to the points of the inset of Fig. 11; T marks the point of the phase transition between the cd and the β -tin phase, see text.

The condition of local stability is fulfilled along all curves shown in Fig. 12. Thus, the volume vs. pressure curves are strictly monotonically decreasing and the enthalpy vs. pressure curves are convex. The condition of global stability requires the enthalpy to be minimal, and so the curves from A to T and from T to F mark the globally stable regime. The point of the phase transition in analogy to the Maxwell construction is noted as

T. The pressure range of the coexistence regime is determined by the overlap of the globally stable and the unstable regions, which is here from B (or D) to E (or C).

A similar picture could be drawn for the $Imma \rightarrow sh$ transition, but with less resolution. A reliable identification of the structures within the $H(p)$ curve analogous to Fig. 12 requires a finer grid of data points for the interpolation and/or a higher convergence.

The enthalpy barrier for the cd \rightarrow β -tin phase transition can be determined with a procedure like illustrated in Fig. 9. In Figs. 13 and 14, we show the enthalpy at given pressures calculated within GGA as a function of the reaction coordinate b/a , for Si and Ge, respectively.

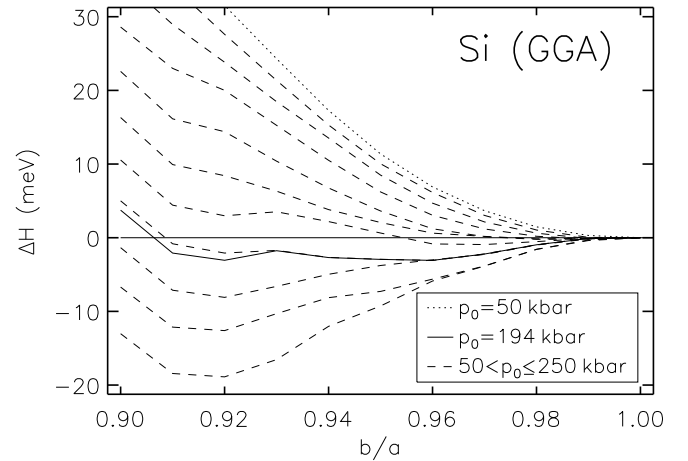


FIG. 13: Enthalpy difference at constant average pressure vs. reaction coordinate b/a , see Eq. (7) for Si. The pressure interval between the dashed lines is 20 kbar. The solid line marks the transition pressure found here.

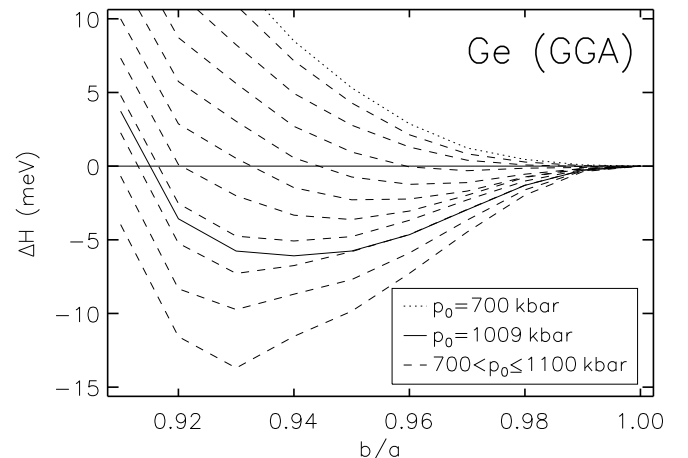


FIG. 14: Same as Fig. 13 but for Ge. The pressure interval between the dashed lines is 40 kbar. The solid curve marks the line corresponding to the transition pressure for the $Imma \rightarrow sh$ transition obtained in Section V.

The enthalpy in Figs. 13 and 14 is reduced by the value

at $b/a = 1$ (corresponding to the β -tin phase),

$$\Delta H(b/a) = H(b/a) - H(1) . \quad (7)$$

The dotted line in Fig. 13 corresponds to a pressure where the enthalpy has a local minimum for the β -tin phase. At a pressure of about 130 kbar we find a continuous transition to the *Imma* phase. Above this pressure, a minimum appears at $b/a < 1$. By further increasing p_0 a second minimum appears at $b/a \sim 0.92$, corresponding to the sh phase. At the pressure of 194 kbar the two minima have the same enthalpy, therefore a transition can occur. The enthalpy barrier between the two phases is surprisingly small, namely 1.2 meV. At higher pressure the sh phase is stable. For the LDA calculation a transition pressure of 133 kbar and an enthalpy barrier of 1.3 meV are obtained. If one considers the enthalpy curves of Fig. 13 at the transition pressures determined in the Sections IV and V, one can give a further estimate of the enthalpy barriers, and, the values obtained following this procedure do not differ appreciably from the ones mentioned above.

As can be seen in Fig. 14 for Ge, a minimum of the enthalpy can be identified corresponding to a pure *Imma* phase, slightly below 820 kbar. However, within our resolution (about 0.1 meV) the pressure curves have only one minimum. Therefore, an enthalpy barrier between the *Imma* and the sh phase can not be identified. Indeed, this transition is of first order. Hence, the existing barrier must be smaller than 0.1 meV.

All the enthalpy barriers which we are able to obtain for the *Imma*→sh transition are much smaller than the thermal energy at room temperature (25 meV). Thus, experiments performed at room temperature should not be able to distinguish between a first- or a second-order phase transition.

VII. DISCUSSION OF THE RESULTS FOR THE PHASE TRANSITIONS

The transition pressures for the $cd \rightarrow \beta$ -tin \rightarrow *Imma* \rightarrow sh phase transitions have been calculated with different methods in the previous sections. In Sections IV and VI an estimate of the hysteresis range was given by considering the relaxed values (R) and the hydrostatic line (HL) respectively. In Section V the transition pressure was determined via the enthalpy vs. pressure curves (EC). In Table IV an overview of all our results for the transition pressure is given in comparison with the experimental results.

For Si the value of the pressure for the $cd \rightarrow \beta$ -tin transition calculated with GGA is within the range of the experimental values whereas the LDA calculation underestimates it. We could not reproduce the experimentally observed hysteresis² for the β -tin \rightarrow *Imma* transition in Si. For a first-order phase transitions, such as *Imma* \rightarrow sh, a hysteresis could occur due to the behaviour of the hydrostatic line as in Fig. 11. Since our results support

TABLE IV: Summary of the estimated transition pressures (p_t) between the cd, β -tin, *Imma*, and sh phase for increasing (\uparrow) and decreasing (\downarrow) pressure, determined by the enthalpy curves (EC), the relaxation (R), and the hydrostatic line (HL).

Si	Method		p_t (kbar)		
$cd \rightarrow \beta$ -tin	EC		121		
	EC		79		
			exp^a		(\uparrow) 103–133
β -tin \leftrightarrow <i>Imma</i>	R	GGA	($\uparrow\downarrow$)	104–109	
	EC	GGA		108	
	R	LDA	($\uparrow\downarrow$)	66–71	
	EC	LDA		71	
			exp^b		(\uparrow) 134–148 127–131 (\downarrow)
<i>Imma</i> \leftrightarrow sh	R	GGA	(\uparrow)	197–198	186–191 (\downarrow)
	HL	GGA	(\uparrow)	198	169 (\downarrow)
	EC	GGA		189	
	R	LDA	(\uparrow)	133–138	131 (\downarrow)
	HL	LDA	(\uparrow)	133	109 (\downarrow)
	EC	LDA		127	
			exp^b		(\uparrow) 149–154 140–157 (\downarrow)
Ge	Method		p_t (kbar)		
$cd \rightarrow \beta$ -tin	EC		96		
	exp^c		(\uparrow)	103–110	
β -tin \leftrightarrow <i>Imma</i>	R	GGA	($\uparrow\downarrow$)	750–763	
	EC	GGA		765	
			exp^d		(\uparrow) 750
<i>Imma</i> \leftrightarrow sh	R	GGA	(\uparrow)	1032	1029–1031 (\downarrow)
	HL	GGA	(\uparrow)	1010	965 (\downarrow)
	EC	GGA		1009	
	exp^d		(\uparrow)	> 810	

^aRefs. 1,2,30,31,33,49,50,51.

^bRef. 2.

^cRefs. 31,38,44,49,50,52.

^dRefs. 3,4.

a second-order phase transition for β -tin \rightarrow *Imma* rather than a first-order one, no hysteresis should be found in this case. The transition pressures mentioned in Ref. 2 are obtained either from the first appearance of a new phase or from the complete transition of the sample from one phase to the other. Thus we estimate the experimental range in which the β -tin \rightarrow *Imma* and *Imma* \rightarrow sh transitions occur in analogy to the procedure explained in Section IV. Unfortunately, the calculated transition pressures for β -tin \rightarrow *Imma* lie below the ones for the first $cd \rightarrow \beta$ -tin phase transition and underestimate the experimental ones.

The next phase transition to be considered is *Imma* \rightarrow sh. Here a hysteresis was found within our calculations as well as in the experiment. The results for the transition pressures within LDA underestimate again the experimental ones, whereas the ones within GGA over-

estimate them. Not included in Table IV are the experimental pressures for mixed (50:50) *Imma*-sh samples, which are 154 kbar for pressure increase and 159 kbar for pressure decrease². This is the only case in which the transition to the (mixed) *Imma* phase occur at a lower pressure for an increasing than for a decreasing external pressure. All other experimental points show the same kind of hysteresis which is reproduced in our results. The difference of the pressures, where the *Imma* phase was measured with pressure increase and decrease is 5 kbar for the mixed samples and 11–12 kbar for the pure ones. From the experimental transition pressures the hysteresis is found to be between 3 and 14 kbar. Within our results the largest possible hysteresis is found to be around 29 (24) kbar and the smallest around 1–12 (2–7) kbar for GGA (LDA), which is in agreement with the experimental values. The transition pressures determined by the crossing of the enthalpy curves are found to be within the hysteresis range calculated here.

For Ge the transition pressure for the *cd*→ β -tin transition is slightly smaller than the experimental one but the results for the β -tin→*Imma* transition match much better. In the experiment^{3,4} just the β -tin→*Imma* transition was examined, because the transition pressure for the *Imma*→sh transition was higher than the maximum accessible pressure of 810 kbar. In comparison to the experimental results of Si it is assumed that the *Imma* phase for Ge is stable from 750 to 850 kbar, which is compatible with the observation of a sh phase at 900 kbar.³⁹ From this point of view, the transition pressure calculated here is slightly too high.

There are many reasons for the discrepancy between our results and the experimental ones. On one hand, the experimental conditions like pressure profiles or measurement times are not perfectly controlled, whereas nonhydrostatic conditions affect the transition pressures; on the other hand, temperature effects, which are neglected in our calculation, could be of some relevance. In fact, for Si the theoretical transition pressure decreases with increasing temperature.⁵³

VIII. CONCLUSIONS

We have presented a first-principles investigation of the pressure-induced phase transitions *cd*→ β -tin→*Imma*→sh in Si and Ge. Numerical accuracy has required these calculations to be performed within the same unit cell and the pressure to be calculated from the stress tensor instead of using any equation of state. We have determined the phase transitions by investigating the relaxed parameters, the enthalpy vs. pressure curves, and the hydrostatic condition. From the pressure dependence of the relaxed structure parameters the hysteresis effect does not seem to have been verified in a theoretical investigation before. An examination of the hydrostatic condition provides a thermodynamical explanation for the existence of this hysteresis. Further on, the orders of the

phase transitions have been investigated with the helps of the curves of the enthalpy vs. pressure and of the derivative of the enthalpy vs. pressure. For Si the transitions *Imma*→sh and β -tin→*Imma* are found to be of first and of second order, respectively. For Ge the results support a second-order β -tin→*Imma* transition more than a first-order one, but in this case the order cannot be definitely determined. A calculation of the enthalpy barriers between the phases show a vanishing barrier between the β -tin and the *Imma* phase for Si, which also supports the second-order β -tin→*Imma* transition, whereas no barrier could be found for all β -tin→*Imma*→sh transitions. Finally, our alternative results are fully consistent with each other and show an acceptable agreement with the available experimental data.

Acknowledgement

Support by the Heinrich Böll Stiftung, Germany, is gratefully acknowledged.

APPENDIX A: FERMI ENERGY AND BAND STRUCTURE

We examined the volume dependence of the Fermi energy of BCT, BCO, and SH. In Fig. 15 we show the Fermi energy reduced by the BCO values for Ge,

$$\Delta E_F(V) = E_F(V) - E_F^{\text{BCO}}(V) \quad . \quad (\text{A1})$$

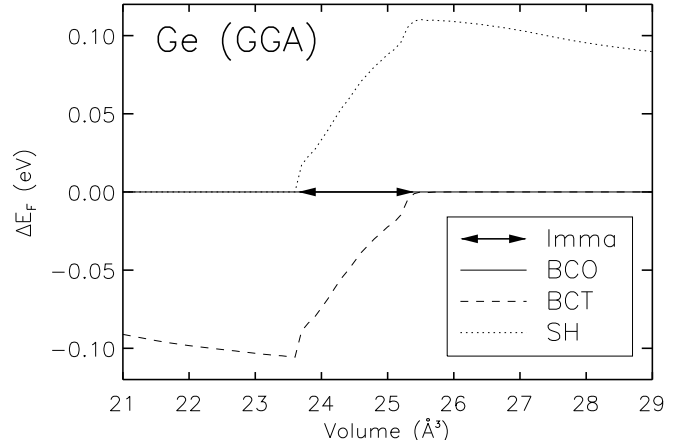


FIG. 15: Fermi energies of the involved structures for Ge reduced by the Fermi energy of BCO, taken as zero.

In the range of stability of the β -tin phase the Fermi energy of BCO is identical with the one of BCT. Similarly, the Fermi energy of BCO and SH are identical in the range of stability of the sh phase. Therefore, the regime where the Fermi energy of BCO is neither equal to the one of BCT nor to the one of SH is assumed here to be the range of stability of the pure *Imma* phase.

We analysed the volume dependence of the band structure for the BCT, BCO, and SH structure, too. The results for the lowest four bands at the Γ -point for Ge are displayed in Fig. 16.

The energy values E_i are reduced in such a way that the Fermi energy at any volume is set equal to zero,

$$\Delta E(V) = E_i(V) - E_F(V) \quad . \quad (\text{A2})$$

In most of the volume range presented in Fig. 16 the band structure presents a linear dependence on volume. However, the energy gradients differ for each structure. Within the transition region between the *Imma* and the sh phase one observes a small discontinuity (here apparent at $V = 23.64\text{\AA}^3$) which is attributed to the first-order phase transition. When starting from the β -tin phase, a deviation of the BCO band energies from the BCT energies can be observed, which increases continuously. Thereby, the degeneracy of the BCT bands is lifted, which indicates the appearance of the less symmetrical *Imma* phase. The behavior of the band structure for Si is very similar to the one of Ge.

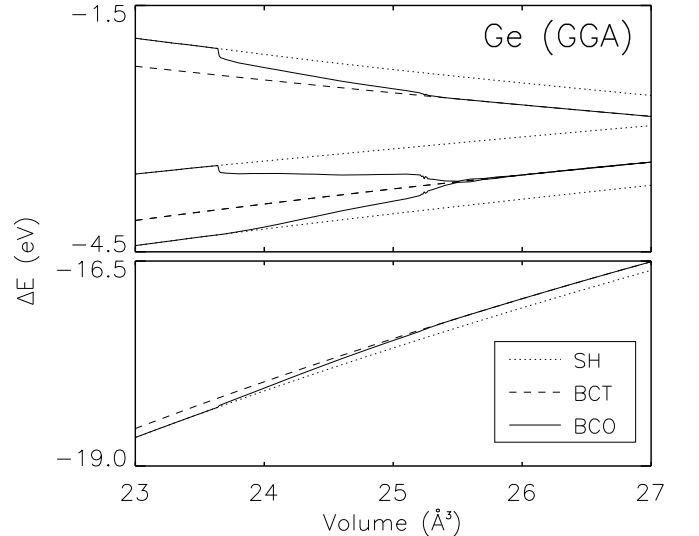


FIG. 16: Eigenenergies at the Γ point, reduced by the Fermi energy for the BCO, BCT and SH structure for Ge.

- ¹ M. I. McMahon and R. J. Nelmes, Phys. Rev. B **47**, 8337 (1993).
- ² M. I. McMahon, R. J. Nelmes, N. G. Wright, and D. R. Allan, Phys. Rev. B **50**, 739 (1994).
- ³ R. J. Nelmes, H. Liu, S. A. Belmonte, J. S. Loveday, M. I. McMahon, D. R. Allan, D. Hausermann, and M. Hanfland, Phys. Rev. B **53**, R2907 (1996).
- ⁴ M. I. McMahon and R. J. Nelmes, Phys. Status Solidi(b) **198**, 389 (1996).
- ⁵ R. J. Needs and R. M. Martin, Phys. Rev. B **30**, 5390 (1984).
- ⁶ S. P. Lewis and M. L. Cohen, Solid State Commun. **89**, 483 (1994).
- ⁷ S. P. Lewis and M. L. Cohen, Phys. Rev. B **48**, 16144 (1993).
- ⁸ M. T. Yin and M. L. Cohen, Phys. Rev. B **26**, 5668 (1982).
- ⁹ N. E. Christensen, D. L. Novikov, R. E. Alonso, and C. O. Rodriguez, Phys. Stat. Sol. (b) **211**, 5 (1999).
- ¹⁰ F. J. Ribeiro and M. L. Cohen, Phys. Rev. B **62**, 11388 (2000).
- ¹¹ M. Hebbache, M. Mattesini, and J. Szeftel, Phys. Rev. B **63**, 205201-1 (2001).
- ¹² N. Boccara, Ann. Phys. (N.Y.) **47**, 40 (1968).
- ¹³ P. Hohenberg and W. Kohn, Phys. Rev. **136**, B864 (1964).
- ¹⁴ W. Kohn and L. J. Sham, Phys. Rev. **140**, A1133 (1965).
- ¹⁵ G. Kresse and J. Furthmüller, Comp. Mat. Sci. **6**, 15 (1996).
- ¹⁶ J. P. Perdew and Y. Wang, Phys. Rev. B **45**, 13244 (1992).
- ¹⁷ J. P. Perdew and A. Zunger, Phys. Rev. B **23**, 5048 (1981).
- ¹⁸ D. M. Ceperley and B. J. Alder, Phys. Rev. Lett. **45**, 566 (1980).
- ¹⁹ D. Vanderbilt, Phys. Rev. B **32**, 8412 (1985).
- ²⁰ G. Kresse and J. Hafner, J. Phys. Cond. Matter **6**, 8245 (1994).
- ²¹ P. Pulay, Chem. Phys. Lett. **73**, 393 (1980).
- ²² H. J. Monkhorst and J. K. Pack, Phys. Rev. B **13**, 5188 (1976).
- ²³ M. Methfessel and A. T. Paxton, Phys. Rev. B **40**, 3616 (1989).
- ²⁴ W. H. Press, B. P. Flannery, S. A. Teukolsky, and W. T. Vetterling, Numerical Recipes, Cambridge University Press, New York (1986).
- ²⁵ M. P. Teter, M. C. Payne, and D. C. Allan, Phys. Rev. B **40**, 12255 (1989).
- ²⁶ D. M. Bylander, L. Kleinman, and S. Lee, Phys. Rev. B **42**, 1394 (1990).
- ²⁷ P. Vinet, J. Ferrante, J. H. Rose, and J. R. Smith, J. Phys. C **19**, L467 (1986).
- ²⁸ F. D. Murnaghan, Proc. Nat. Acad. Sci. **30**, 244 (1944).
- ²⁹ K. Gaal-Nagy and D. Strauch, submitted to Comp. Mat. Sci.
- ³⁰ J. Z. Hu, L. D. Merkle, C. S. Menoni, and I. L. Spain, Phys. Rev. B **34**, 4679 (1986).
- ³¹ H. Olijnyk, S. Sikka, and W. B. Holzapfel, Phys. Lett **103A**, 137 (1984); J. Phys. (Paris) **45**, Suppl. Colloq. C8, C8-153 (1984).
- ³² J. C. Jamieson, Science **139**, 762 (1963).
- ³³ J. Z. Hu and I. L. Spain, Solid State Commun. **51**, 263 (1984).
- ³⁴ S. J. Duclos, Y. K. Vohra, and A. L. Ruoff, Phys. Rev. B **41**, 12021 (1990).
- ³⁵ M. Hanfland, U. Schwarz, K. Syassen, and K. Takemura, Phys. Rev. Lett. **82**, 1197 (1999).
- ³⁶ M. A. Baublitz and A. L. Ruoff, J. Appl. Phys. **53**, 5669 (1982).
- ³⁷ S. B. Quadri, E. F. Skelton, and A. W. Webb, J. Appl. Phys. **54**, 3609 (1983).
- ³⁸ C. S. Menoni, J. Z. Hu, and I. L. Spain, Phys. Rev. B **34**, 362 (1986).
- ³⁹ Y. K. Vohra, K. E. Brister, S. Desgreniers, A. L. Ruoff, K. J. Chang, and M. L. Cohen, Phys. Rev. Lett. **56**, 1944 (1986).

⁴⁰ A. Bergamin, G. Cavagnero, G. Mana, and G. Zosi, Eur. Phys. J. B **9**, 225 (1999).

⁴¹ G. Basile, A. Bergamin, G. Cavagnero, G. Mana, E. Vittone, and G. Zosi, Phys. Rev. Lett. **72**, 3133 (1994).

⁴² H. Holloway, K. C. Hass, M. A. Tamor, T. R. Anthony, and W. F. Banholzer, Phys. Rev. B **44**, 7123 (1991).

⁴³ D. Windisch and P. Becker, Phys. Status Solidi (a) **118**, 379 (1991).

⁴⁴ A. Yoshiasa, K. Koto, H. Maeda, and T. Ishii, Jpn. J. Appl. Phys. **36**, 781 (1997).

⁴⁵ A. S. Cooper, Acta Crystallogr. **15**, 578 (1962).

⁴⁶ G. Mills, H. Jónsson, and K. Schenter, Surf. Sci. **324**, 305 (1995).

⁴⁷ H. Jónsson, G. Mills, and K. W. Jacobson, in Classical and Quantum Dynamics in Condensed Phase simulations, ed. by B. J. Berne, G. Ciccotti, and D. F. Cother (World Scientific, 1998).

⁴⁸ K. Gaal-Nagy, A. Bauer, P. Pavone, and D. Strauch, submitted to Comp. Mat. Sci.

⁴⁹ A. Werner, J. A. Sanjurjo, and M. Cardona, Solid State Commun. **44**, 155 (1982).

⁵⁰ I. L. Spain, J. Z. Hu, C. S. Menoni, and D. Black J. Phys. (Paris) **45** Suppl. Colloq. C8, C8-407 (1984).

⁵¹ Y. X. Zhao, F. Buehler, J. R. Sites, and I. L. Spain, Solid State Commun. **59**, 679 (1986).

⁵² A. Polian, J. P. Itié, C. Jaubertie-Carillon, A. Dartige, A. Fontaine, and H. Tolentino, High Pressure Res. **4**, 309 (1990).

⁵³ K. Gaal-Nagy, M. Schmitt, P. Pavone, and D. Strauch, Comp. Mat. Sci. **22**, 49 (2001).